Journal of King Saud University – Science 31 (2019) 114–126

Contents lists available at ScienceDirect

Journal of King Saud University – Science

journal homepage: www.sciencedirect.com

Original article

Integral transform solution of micropolar magnetohydrodynamic oscillatory flow with heat and mass transfer over a plate in a porous medium subjected to chemical reactions

Fabio A. Pontes [a], Helder K. Miyagawa [a], Péricles C. Pontes [b,c], Emanuel N. Macêdo [a,d], João N.N. Quaresma [a,d,*]

[a] Graduate Program in Natural Resource Engineering in the Amazon, PRODERNA/ITEC/UFPA, Universidade Federal do Pará, 66075-110 Belém, PA, Brazil
[b] Dept. of Mechanical Engineering, COPPE/UFRJ, Universidade Federal do Rio de Janeiro, Cx. Postal 68503, Cidade Universitária, Rio de Janeiro, RJ 21945-970, Brazil
[c] Araguaia Institute of Engineering, IEA/UNIFESSPA, Universidade do Sul e Sudeste do Pará, Campus Santana do Araguaia, Bel Recanto, Rua Albino Malzoni, 68560-000 Santana do Araguaia, PA, Brazil
[d] School of Chemical Engineering, FEQ/ITEC/UFPA, Universidade Federal do Pará, Campus Universitário do Guamá, 66075-110 Belém, PA, Brazil

ARTICLE INFO

Article history:
Received 18 May 2017
Accepted 7 July 2017
Available online 10 July 2017

Keywords:
Generalized Integral Transform Technique (GITT)
Equations of Motion
Magnetohydrodynamic (MHD)
Heat and mass transfer
Porous Medium
Chemical reaction

ABSTRACT

The main goal of the present work is to show the procedure, application and main features of the hybrid numerical-analytical approach known as GITT (Generalized Integral Transform Technique) by solving an unsteady, one-dimensional magnetohydrodynamic (MHD) oscillatory flow of a micropolar and incompressible fluid with heat and mass transfer through a permeable vertical plate embedded in a porous medium in the presence of chemical reaction. The mathematical formulation of the studied model was obtained from the equation of motion and the mass and energy balances by considering laminar and incompressible flow subjected to a constant transverse magnetic field with constant physical properties. Convergence analysis was performed and presented to illustrate the consistency of the integral transform technique. Linear and angular velocities distribution, temperature and concentration profiles were generated and numerically verified with an approximate solution found in the literature and with the results of the method of lines (MOL) with good agreement. The effects of some governing parameters, namely, dimensionless time, magnetic field parameter, Schmidt and Prandtl numbers, permeability and chemical reaction parameters, on these fields were presented. The effects of these parameters on the local skin friction coefficient, the couple stress coefficient, the local Nusselt number and the local Sherwood number were also critically evaluated. Therefore, results show that the linear velocity decreases with increasing magnetic field parameter, while the angular velocity increases with increasing the same and the linear and angular velocities and the concentration field decrease as the Schmidt number increases while the temperature field decreases with increasing Prandtl number.

1. Introduction

1.1. Introductory section

Magnetohydrodynamic (MHD) is the study of the interaction between the electromagnetic and velocity fields of conductive fluids. Its mathematical modeling is characterized by a coupling between the fluid mechanics equations and Maxwell's equations of electromagnetism. The interest in magnetohydrodynamics began to emerge in the early twentieth century and, from the 1960s until now, these studies have received considerable attention due mainly to energy and environmental issues. Magnetohydrodynamic flow can be found in channels with heat transfer

* Corresponding author Graduate Program in Natural Resource Engineering in the Amazon, PRODERNA/ITEC/UFPA, Universidade Federal do Pará, 66075-110, Belém, PA, Brazil.
E-mail address: quaresma@ufpa.br (J.N.N. Quaresma).
Peer review under responsibility of King Saud University.

Production and hosting by Elsevier

http://dx.doi.org/10.1016/j.jksus.2017.07.002
1018-3647/

Nomenclature

A_{ij}	Integral transform coefficient defined by Eq. (19)
B_0	Constant magnetic field applied externally
$C(y^*,t^*)$	Fluid concentration
C_f	Local skin friction factor
c_p	Specific heat at constant pressure
C'_w	Local couple stress coefficient
C_w	Wall concentration
C_∞	Free stream concentration
D	Molecular diffusivity
G_{rT}	Thermal Grashof number
G_{rC}	Mass Grashof number
j	Dimensionless micro-inertia per unit mass
j^*	Micro-inertia per unit mass
k	Thermal conductivity
K	Permeability parameter
K_1	Dimensionless permeability parameter defined by Eq. (3s)
L	Sufficiently large value of y where the velocity profile u approaches U_0
M	Magnetic field parameter defined by Eq. (3n)
M_w	Wall couple stress
n	Frequency parameter defined by Eq. (3j)
n_1	Parameter related to micro-rotation vector and shear stress
N_i	Normalization integral of the eigenfunction defined by Eq. (12e)
Nu	Local Nusselt number
$NuRe_x^{-1}$	Heat transfer rate at the surface defined by Eq. (26)
N	Truncation order for the eigenfunction expansion
NPT	Number of points for the mesh MOL
Pr	Prandtl number
Re_x	Local Reynolds number
Sc	Schmidt number
Sh	Local Sherwood number
$ShRe_x^{-1}$	Mass transfer rate at the surface defined by Eq. (27)
$T(y^*,t^*)$	Fluid temperature
T_w	Wall temperature
T_∞	Free stream temperature
t^*	Time
t	Dimensionless time
$u(y,t)$	Dimensionless linear velocity
$\bar{u}_{h,i}(t)$	Transformed potential for the linear velocity field
$u_p{}^*$	Fluid uniform velocity in its own plane
U_p	Dimensionless plate velocity
U_0	Free stream velocity
V_0	Scale of suction velocity at the plate
x,y	Dimensionless spatial coordinates
x^*,y^*	Spatial coordinates

Greek Letters

α	Thermal diffusivity
β	Dimensionless viscosity ratio
β_C	Coefficient of fluid mass expansion
β_T	Coefficient of fluid thermal expansion
γ	Spin gradient viscosity
$\gamma_1{}^*$	Reaction rate constant
γ_1	Dimensionless chemical reaction parameter defined by Eq. (3t)
Δy	Step size
ε	Small positive quantity
η	Similarity variable defined by Eq. (3h)
$\theta(y,t)$	Dimensionless temperature
$\bar{\theta}_{h,i}(t)$	Transformed potential for the temperature field
Λ	Coefficient of vortex viscosity
μ	Dynamic viscosity of the fluid
μ_i	Eigenvalue defined by Eq. (12b)
ν	Fluid kinematics viscosity
ν_r	Kinematic rotational viscosity
ρ	Fluid density
σ	Fluid electrical conductivity
$\tau_w{}^*$	Wall shear stress
$\phi\ (y,t)$	Dimensionless concentration
$\bar{\phi}_{h,i}(t)$	Transformed potential for the concentration field
ψ_i	Eigenfunction defined by Eq. (12a)
$\tilde{\psi}_i$	Normalized eigenfunction defined by Eq. (15)
$\omega(y,t)$	Dimensionless angular velocity
$\bar{\omega}_{h,i}(t)$	Transformed potential for the angular velocity field

Subscripts and Superscripts

*	Dimensional variables
i,j,k	Eigenvalues order
i	Number of points in the discrete domain of the MOL approach
h	Filtered problem
p	Particular problem

including pumps and MHD generators, cooling systems of nuclear reactors and electrolytic reduction cells in aluminum plants (Shercliff, 1965; Davidson, 2001; Sutton and Sherman, 2006). To extract the maximum benefit from magnetohydrodynamic flow, a better understanding of the phenomenon is important. The importance of the study of magnetohydrodynamic flow is highlighted by the recent introduction of numerical kernels solvers for Maxwell's equations in the beta versions of major CFD commercial packages that automatically couple to the CFD solvers (Ansys/CFX, 2009).

Eringen (1966) originally developed the theory of micropolar fluids, which has recently become a popular field of research since the Navier-Stokes equations do not describe the properties of polar fluid, colloidal solutions, suspensions, liquid crystals, fluids containing small additives, etc. The concept of micropolar fluid describes the effects of micro-rotation in microstructures and addresses a class of fluids that exhibits certain microscopic effects arising from the micro-motions of the fluid elements.

At the same time, there is a growing need for the development and application of mathematical methods that are as analytical in nature as possible to solve models in various science fields. Among the methodologies that satisfy this condition is the so-called Generalized Integral Transform Technique (GITT), which is able to treat a large number of nonlinear problems and which is an alternative tool for solving this class of problems. This technique is based on the use of orthogonal eigenfunctions expansions to express the unknown dependent variables (Cotta, 1993; Cotta and Mikhailov, 1997; Santos et al., 2001; Sphaier et al., 2011).

Thus, considering the hybrid numerical-analytical nature of the GITT approach and its guarantee of local and global error control, the objective of this work is to show the main characteristics of applying this methodology for solving the one-dimensional magnetohydrodynamic (MHD) oscillating flow of a micropolar incompressible fluid with heat and mass transfer through a permeable vertical plate embedded in a porous medium in the presence of chemical reaction. The method of lines (MOL) will be used also

to allow a numerical verification between these two methodologies. The mathematical models are obtained from the equations of motion along with the mass and energy balances assuming constant physical properties. The flow in the problem is subjected to a constant transverse magnetic field. The convergence behavior of the integral transform was performed to evaluate the influence of the truncation orders in the eigenfunction series expansions. A detailed analysis of effects of the parametric variation of the main dimensionless parameters for some typical situations on the velocities, temperature and concentration profiles, as well as on the local skin friction coefficient, couple stress coefficient, local Nusselt number and local Sherwood number was performed. Verification of the integral transform results has been performed by comparing them with those of Modather et al. (2009) and the MOL approach.

1.2. Literature review

Micropolar fluids contain dilute suspension of rigid macromolecules with individual motions that support stress and body moments that are influenced by spin inertia. These fluids contain micro-constituents that can undergo rotation, which can affect the hydrodynamics of the flow such that it can be distinctly non-Newtonian. Thus, micropolar fluids consist of randomly oriented particles that are suspended in a viscous fluid and which can undergo a rotation (Eringen, 1966). The fundamentals of micropolar fluids have been investigated substantially over the years (Babu et al., 2013; Gupta et al., 2014; Sheikh et al., 2017).

Babu et al. (2013) analyzed the effects of mass transfer on the unsteady MHD convective flow of a micropolar fluid past a vertical moving porous plate through a porous medium with viscous dissipation. They noted that the velocity distribution greater for a Newtonian fluid with given parameters, as compared with micropolar fluids until its peak value reaches. They also observed that the effect of increasing values of magnetic field parameter results in a decreasing velocity distribution across the boundary layer. Gupta et al. (2014) examined unsteady mixed convection flow of a micropolar fluid over a porous shrinking sheet using a variational finite element method. For limiting cases, the numerical results obtained for the flow velocity compared very well with the exact solution available in the literature and the numerical simulations clearly demonstrated that the drag can be reduced effectively by the prudent selection of the studied parameters. Sheikh et al. (2017) analyzed the MHD flow of micropolar fluid past an oscillating infinite vertical plate embedded in a porous media. The authors applied the Laplace transform technique to obtain the exact solutions for velocity, temperature, and concentration fields, as well the corresponding skin friction and wall couple stress. They observed that an increase in magnetic field reduces the fluid velocity and magnitude of microrotation, while velocity and magnitude of microrotation are directly related to permeability parameter that causes fall in drag forces. They also commented that velocity and magnitude of microrotation decrease as Prandtl number is increased and the skin friction increases with increase in magnetic field.

The effects of a chemical reaction depend greatly on whether the reaction is heterogeneous or homogeneous and the reaction order. A destructive reaction occurs when the chemical reaction parameter (γ_1) is positive, while in a generative reaction, this parameter is negative. Since in many industrial processes the diffusing species may be generated or absorbed due to chemical reaction, the reaction can highly affect the flow and therefore the properties of the final product. Several studies have assessed the influence of the chemical reaction parameter (Al-Odat and Al-Azab, 2007; Pal and Talukdar, 2010a; Bég et al., 2016).

The effects of chemical reaction on transient MHD free convection over a moving vertical plate were investigated by Al-Odat and Al-Azab (2007) and they observed that the velocity as well as the concentration decrease with increasing chemical reaction parameter. Unsteady magnetohydrodynamic convective heat and mass transfer in a boundary layer slip flow past a vertical permeable plate with thermal radiation and chemical reaction were studied by Pal and Talukdar (2010a) and they solved the non-linear coupled partial differential equations employing perturbation analysis. They recorded that the velocity as well as the concentration decrease with increasing chemical reaction parameter. Bég et al. (2016) evaluated the transient MHD heat and mass transfer in chemically-reacting fluid flow from an impulsively-started vertical perforated sheet. The authors solved the model with a finite difference method and verified their solutions with computational codes from a variational finite element method and also from a network simulation method.

The basic problem of flow through and past porous media has been studied extensively over the past few years, both theoretically and experimentally (Pal and Talukdar, 2010b; Acharya et al., 2014). The buoyancy and chemical reaction effects on MHD mixed convection heat and mass transfer in a porous medium with thermal radiation and Ohmic heating was investigated by Pal and Talukdar (2010b) and they found that the presence of a porous medium increases the skin friction coefficient, whereas increasing the porous permeability decreases the local Nusselt number. Free convective fluctuating MHD flow through porous media past a vertical porous plate with variable temperature and a heat source was evaluated by Acharya et al. (2014) and they concluded that the presence of the porous media has no significant contribution to the flow characteristics, whereas viscous dissipation compensates for the heating and cooling of the plate due to the convective current.

Free convection flow with a magnetic field has been evaluated by many authors (Prasad et al., 2013; Vija et al., 2014). Prasad et al. (2013) investigated the effects of internal heat generation/absorption, thermal radiation, magnetic field, variable fluid property and viscous dissipation on the heat transfer characteristics of a Maxwell fluid over a stretching sheet, and they have noted that the horizontal velocity decreases with increasing magnetic field, and this is because the transverse magnetic field has a tendency to create a drag-like force, known as the Lorentz force, to resist the flow. The influence of induced magnetic field and viscous dissipation on MHD mixed convective flow past a vertical plate in the presence of thermal radiation was analyzed by Vija et al. (2014) and they recorded that the values of the induced magnetic field remained negative, i.e., induced magnetic flux reversal arises for all distances in the boundary layer.

The Generalized Integral Transform Technique (GITT) considers that any potential can be constructed as an expansion of eigenfunctions. It eliminates the need to find an exact integral transformation that results in an uncoupled ordinary differential system, as traditional analytical approaches usually do, thereby emerging as an alternative to purely numerical methods for the solution of complex engineering problems usually treated only by numerical approaches. This technique has been employed through the years to study various phenomena (Lima et al., 2007; Lima and Rêgo, 2013).

The GITT approach was also employed by Lima et al. (2007) to solve the transient, fully developed, MHD flow and heat transfer of Newtonian fluids inside channels between parallel porous plates where the flow was sustained by a constant pressure gradient. Integral transform results were satisfactorily verified with the literature and the authors found that both the velocity and temperature potentials showed fast convergence, since, for the cases considered, the solution of the original problem is practically obtained by the filter solution.

Lima and Rêgo (2013) also applied GITT to study the dynamics of the steady state, incompressible laminar flow and heat transfer of a Newtonian, electrically conductive fluid at the entrance region of a parallel-plate channel subjected to a uniform external magnetic field. Two types of the velocity field in the entry channel (uniform and parabolic inlet) and one boundary condition for the temperature profile (uniform inlet) were analyzed. Their results were compared with previously reported numerical solutions for different values of the governing parameters and of the entry boundary conditions, obtaining excellent agreement with literature results that applied the finite difference method.

Given the importance of the MHD flow of micropolar fluids, and in view of the potential application of GITT approach to solve nonlinear and coupled models, this work presents an important and innovative solution of the problem of MHD flow with simultaneous mass and energy transfer of a micropolar fluid past a permeable vertical plate embedded in a porous medium in the presence of chemical reaction using the GITT methodology.

2. Mathematical formulation

The problem addressed in this paper is defined by considering the one-dimensional magnetohydrodynamic oscillatory transient laminar flow of a micropolar fluid past a permeable vertical plate embedded in a porous medium in the presence of chemical reaction with heat and mass transfer. The flow arises along the x-axis on a plate which moves continuously at uniform speed, u_p^*, and a constant magnetic field, B_0, is applied in the y direction, neglecting any induced magnetic field. It is assumed that a uniform surface temperature, T_w, is maintained, while the ambient temperature, T_∞, is constant such that $T_w > T_\infty$. A uniform concentration of the species at the surface, C_w, is maintained and the concentration in the ambient fluid is C_∞. The chemical reaction is considered first order and irreversible. The Joule heating and the term due to power dissipation are neglected. Fig. 1 shows the main characteristics of the flow and the geometry of the studied problem.

In the present study, the original problem of a semi-infinite medium has been turned into a finite medium problem. Therefore,

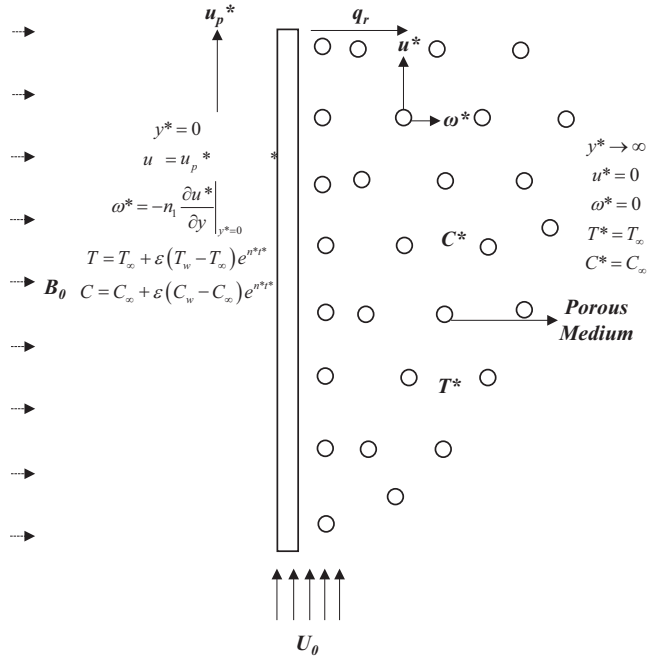

Fig. 1. Geometric representation of the studied problem.

the boundary conditions for $y \to \infty$ is replaced by identical ones at L, which is a sufficiently large value of y that the velocity u approaches the relevant free stream velocity (i.e., $L = 8$).

From the simplifications adopted and using the equations of motion and the energy and mass balances, the governing equations of the flow with heat and mass transfer can be written in dimensionless form as in Modather et al. (2009):

$$\frac{\partial u}{\partial t} - \frac{\partial u}{\partial y} = (1+\beta)\frac{\partial^2 u}{\partial y^2} + 2\beta\frac{\partial \omega}{\partial y} + G_{rT}\theta + G_{rC}\phi - \left(M + \frac{1+\beta}{K_1}\right)u \qquad 0 < y < L, t \geqslant 0 \tag{1a}$$

$$\frac{\partial \omega}{\partial t} - \frac{\partial \omega}{\partial y} = \frac{1}{\eta}\frac{\partial^2 \omega}{\partial y^2} \qquad 0 < y < L, t \geqslant 0 \tag{1b}$$

$$\frac{\partial \theta}{\partial t} - \frac{\partial \theta}{\partial y} = \frac{1}{\mathrm{Pr}}\frac{\partial^2 \theta}{\partial y^2} \qquad 0 < y < L, t \geqslant 0 \tag{1c}$$

$$\frac{\partial \phi}{\partial t} - \frac{\partial \phi}{\partial y} = \frac{1}{Sc}\frac{\partial^2 \phi}{\partial y^2} + \gamma_1 \phi \qquad 0 < y < L, t \geqslant 0 \tag{1d}$$

These equations are subjected to the following initial and boundary conditions:

$$\begin{cases} u(y,0) = f_1(y,0) \\ \omega(y,0) = f_2(y,0) \\ \theta(y,0) = f_3(y,0) \\ \phi(y,0) = f_4(y,0) \end{cases}; \quad \begin{cases} u(0,t) = U_p \\ \omega(0,t) = -n_1 \frac{\partial u}{\partial y}\Big|_{y=0} \\ \theta(0,t) = 1 + \varepsilon e^{nt} \\ \phi(0,t) = 1 + \varepsilon e^{nt} \end{cases}; \quad \begin{cases} u(L,t) = 0 \\ \omega(L,t) = 0 \\ \theta(L,t) = 0 \\ \phi(L,t) = 0 \end{cases} \tag{2a-l}$$

In the formulation given by Eqs. (1) and (2), the following dimensionless groups were employed:

$$u = \frac{u^*}{U_0}; \quad v = \frac{v^*}{V_0}; \quad y = \frac{y^* V_0}{\nu}; \quad U_p = \frac{u_p^*}{U_0}; \quad \omega = \frac{\omega^* \nu}{U_0 V_0};$$
$$t = \frac{t^* V_0^2}{\nu}; \quad \theta = \frac{T - T_\infty}{T_w - T_\infty}; \quad \eta = \frac{2}{2+\beta}; \quad \phi = \frac{C - C_\infty}{C_w - C_\infty};$$
$$n = \frac{n^* \nu}{V_0^2}; \quad j = \frac{j^* V_0^2}{\nu^2}; \quad Pr = \frac{\nu}{\alpha} = \frac{\mu c_p}{k}; \quad Sc = \frac{\nu}{D};$$
$$M = \frac{\sigma B_0^2 \nu}{\rho V_0^2}; \quad G_{rT} = \frac{\nu g \beta_T (T_w - T_\infty)}{U_0 V_0^2}; \quad G_{rC} = \frac{\nu g \beta_C (C_w - C_\infty)}{U_0 V_0^2};$$
$$\gamma = \left(\mu + \frac{\Lambda}{2}\right); \quad j^* = \mu j^* \left(1 + \frac{\beta}{2}\right); \quad \beta = \frac{\Lambda}{\mu} = \frac{\nu_r}{\nu}; \quad K_1 = \frac{K U_0 V_0^2}{\nu^2};$$
$$\gamma_1 = \frac{\nu \gamma_1^*}{V_0^2 V} \tag{3a-t}$$

The initial conditions were obtained from the work of Modather et al. (2009) by applying $t = 0$ in their approximate solutions. Such approximate solutions are as shown in the following equations:

$$f_1(y,t) = a_1 e^{-h_2 y} + a_2 e^{-\mathrm{Pr} y} + a_4 e^{-h_5 y} + a_3 e^{-\eta y} + \varepsilon\left(b_1 e^{-h_1 y} + b_2 e^{-h_3 y} + b_3 e^{-h_4 y} + b_4 e^{-h_6 y}\right)e^{nt} \tag{4a}$$

$$f_2(y,t) = c_1 e^{-\eta y} + \varepsilon(c_2 e^{-h_1 y})e^{nt}; \quad f_3(y,t) = e^{-\mathrm{Pr} y} + \varepsilon\left(e^{-h_4 y}\right)e^{nt};$$
$$f_4(y,t) = e^{-h_5 y} + \varepsilon\left(e^{-h_6 y}\right)e^{nt} \tag{4b-d}$$

$$h_1 = \frac{\eta}{2}\left[1 + \sqrt{1 - \frac{4n}{\eta}}\right];$$
$$h_2 = \frac{1}{2(1+\beta)}\left[1 + \sqrt{1 + 4\left(M + \frac{1+\beta}{K_1}\right)(1+\beta)}\right] \tag{4e,f}$$

$$h_3=\frac{1}{2(1+\beta)}\left[1+\sqrt{1-4(n-M-\frac{1+\beta}{K_1})(1+\beta)}\right];$$
$$h_4=\frac{Pr}{2}\left[1+\sqrt{1-\frac{4n}{Pr}}\right] \quad (4g,h)$$

$$h_5=\frac{Sc}{2}\left[1+\sqrt{1-\frac{4\gamma_1}{Sc}}\right];\quad h_6=\frac{Sc}{2}\left[1+\sqrt{1-\frac{4(n+\gamma_1)}{Sc}}\right] \quad (4i,j)$$

$$a_1=U_p-a_2-a_3-a_4;\quad a_2=-\frac{G_{rT}}{(1+\beta)Pr^2-Pr-(M+\frac{1+\beta}{K_1})} \quad (4k,l)$$

$$a_3=\frac{2\beta\eta}{(1+\beta)\eta^2-\eta-\left(M+\frac{1+\beta}{K_1}\right)}c_1=\lambda c_1;$$
$$a_4=-\frac{G_{rC}}{(1+\beta)h_5^2-h_5-\left(M+\frac{1+\beta}{K_1}\right)} \quad (4m,n)$$

$$b_1=\frac{2\beta h_1}{(1+\beta)h_1^2-h_1+\left(n-M-\frac{1+\beta}{K_1}\right)}c_2=\xi c_2;\quad b_2=-(b_1+b_3+b_4) \quad (4o,p)$$

$$b_3=-\frac{G_{rT}}{(1+\beta)h_4^2-h_4+\left(n-M-\frac{1+\beta}{K_1}\right)};$$
$$b_4=-\frac{G_{rC}}{(1+\beta)h_6^2-h_6+\left(n-M-\frac{1+\beta}{K_1}\right)} \quad (4q,r)$$

$$c_1=\frac{n_1\left[h_2U_p-h_2a_2-h_2a_4+Pra_2+h_5a_4\right]}{1+n_1\lambda(h_2-\eta)};$$
$$c_2=\frac{n_1b_3(h_4-h_3)+n_1b_4(h_6-h_3)}{1+n_1\xi(h_3-h_1)} \quad (4s,t)$$

3. Solution methodology

3.1. Splitting of potentials

In order to improve the GITT performance and accelerate the convergence of the method, a splitting-up procedure is employed to remove the non-homogeneity in the boundary condition at $y=0$. To do this, each original potential, $u(y,t)$, $\omega(y,t)$, $\theta(y,t)$ and $\phi(y,t)$, is split-up as follows:

$$u(y,t)=u_h(y,t)+u_p(y);\quad \omega(y,t)=\omega_h(y,t)+\omega_p(y;t) \quad (5a,b)$$

$$\theta(y,t)=\theta_h(y,t)+\theta_p(y;t);\quad \phi(y,t)=\phi_h(y,t)+\phi_p(y;t) \quad (5c,d)$$

here, $u_p(y)$, $\omega_p(y;t)$, $\theta_p(y;t)$ and $\phi_p(y;t)$ are potentials whose boundary conditions carry the original non-homogeneities at the wall, and $u_h(y,t)$, $\omega_h(y,t)$, $\theta_h(y,t)$ and $\phi_p(y,t)$ are potentials with homogeneous boundary conditions. By applying these definitions to Eqs. (1) subjected to the initial and boundary conditions given by Eqs. (2), the following filtered problems are obtained:

$$\frac{\partial u_h}{\partial t}-\frac{\partial u_h}{\partial y}=(1+\beta)\frac{\partial^2u_h}{\partial y^2}+2\beta\frac{\partial\omega_h}{\partial y}+G_{rT}\theta_h+G_{rC}\phi_h-\left(M+\frac{1+\beta}{K_1}\right)u_h+2\beta\frac{\partial\omega_p}{\partial y}+G_{rT}\theta_p+G_{rC}\phi_p \quad (6a)$$

$$\frac{\partial\omega_h}{\partial t}-\frac{\partial\omega_h}{\partial y}=\frac{1}{\eta}\frac{\partial^2\omega_h}{\partial y^2}-\frac{\partial\omega_p}{\partial t} \quad (6b)$$

$$\frac{\partial\theta_h}{\partial t}-\frac{\partial\theta_h}{\partial y}=\frac{1}{Pr}\frac{\partial^2\theta_h}{\partial y^2}-\frac{\partial\theta_p}{\partial t} \quad (6c)$$

$$\frac{\partial\phi_h}{\partial t}-\frac{\partial\phi_h}{\partial y}=\frac{1}{Sc}\frac{\partial^2\phi_h}{\partial y^2}+\gamma_1\phi_h-\frac{\partial\phi_p}{\partial t} \quad (6d)$$

With the following initial and boundary conditions:

$$\begin{cases}u_h(y,0)=F_1(y)=f_1(y,0)-u_p(y)\\ \omega_h(y,0)=F_2(y)=f_2(y,0)-\omega_p(y;0)\\ \theta_h(y,0)=F_3(y)=f_3(y,0)-\theta_p(y;0)\\ \phi_h(y,0)=F_4(y)=f_4(y,0)-\phi_p(y;0)\end{cases};\quad \begin{cases}u_h(0,t)=0\\ \omega_h(0,t)=0\\ \theta_h(0,t)=0\\ \phi_h(0,t)=0\end{cases};$$
$$\begin{cases}u_h(L,t)=0\\ \omega_h(L,t)=0\\ \theta_h(L,t)=0\\ \phi_h(L,t)=0\end{cases} \quad (7a\text{-}l)$$

The particular problems have been defined as the permanent version of the original equations of each potential, disregarding, in the case of linear velocity, the portions relating to other potentials:

$$\frac{d^2u_p}{dy^2}+\left(\frac{1}{1+\beta}\right)\frac{du_p}{dy}-\left[\frac{1+K_1M+\beta}{K_1(1+\beta)}\right]u_p=0 \quad (8a)$$

$$\frac{d^2\omega_p}{dy^2}+\eta\frac{d\omega_p}{dy}=0 \quad (8b)$$

$$\frac{d^2\theta_p}{dy^2}+Pr\frac{d\theta_p}{dy}=0 \quad (8c)$$

$$\frac{d^2\phi_p}{dy^2}+Sc\frac{d\phi_p}{dy}+(Sc\gamma_1)\phi_p=0 \quad (8d)$$

With the following boundary conditions:

$$\begin{cases}u_p(0)=U_P\\ \omega_p(0;t)=-n_1\left(\frac{\partial u_p}{\partial y}+\frac{\partial u_h}{\partial y}\right)\Big|_{y=0}\\ \theta_p(0;t)=1+\varepsilon e^{nt}\\ \phi_p(0;t)=1+\varepsilon e^{nt}\end{cases};\quad \begin{cases}u_p(L)=0\\ \omega_p(L;t)=0\\ \theta_p(L;t)=0\\ \phi_p(L;t)=0\end{cases} \quad (9a\text{-}h)$$

The solution of the permanent version of the original equations were analytically obtained by numerical-symbolic computing platform *Mathematica 9.0* (Wolfram, 2005), to yield:

$$u_p(y)=\frac{e^{-\frac{y-\frac{y}{\sqrt{K_1}}\sqrt{4(1+\beta)^2+K_1[1+4M(1+\beta)]}}{2(1+\beta)}}\left(e^{\frac{(L-y)\sqrt{4(1+\beta)^2+K_1[1+4M(1+\beta)]}}{\sqrt{K_1}(1+\beta)}}-1\right)}{e^{\frac{L\sqrt{4(1+\beta)^2+K_1[1+4M(1+\beta)]}}{\sqrt{K_1}(1+\beta)}}-1}U_p \quad (10a)$$

$$\omega_p(y;t)=\frac{e^{(L-y)\eta}-1}{e^{L\eta}-1}\left[-n_1\left(\frac{du_p}{dy}\Big|_{y=0}+\frac{\partial u_h}{\partial y}\Big|_{y=0}\right)\right] \quad (10b)$$

$$\theta_p(y;t)=\frac{e^{Pr(L-y)}-1}{e^{PrL}-1}\left(1+\varepsilon e^{nt}\right) \quad (10c)$$

$$\phi_p(y;t)=\frac{e^{-\frac{y}{2}\sqrt{Sc}(\sqrt{Sc}+\sqrt{Sc-4\gamma_1})}\left(e^{L\sqrt{Sc}\sqrt{Sc-4\gamma_1}}-e^{y\sqrt{Sc}\sqrt{Sc-4\gamma_1}}\right)}{e^{L\sqrt{Sc}\sqrt{Sc-4\gamma_1}}-1}\left(1+\varepsilon e^{nt}\right) \quad (10d)$$

The solution for the potential $\omega_p(y;t)$ given by Eq. (10b) is coupled, and will be simultaneously obtained with that for the potential $u_h(y,t)$.

3.2. Integral transform solution

Since all boundary conditions in $y = 0$ are now homogeneous, the integral transformation of Eqs. (6a)–(6d) can be performed. The first step is to choose an eigenvalue problem, which provides the basis for the construction of a desired potential as an expansion of orthogonal eigenfunctions. Such an eigenvalue problem is given by:

$$\frac{d^2\psi_i}{dy^2} + \mu_i^2\psi_i = 0 \tag{11a}$$

$$\psi_i(0) = 0; \qquad \psi_i(L) = 0 \tag{11b, c}$$

The analytical solution for this eigenvalue problem is given by Özisik (1993) as follows:

$$\psi_i(y) = sin(\mu_i y); \qquad \mu_i = \frac{i\pi}{L}; \qquad i = 1, 2, 3, \ldots \tag{12a, b}$$

$$\int_0^L \psi_i(y)\psi_j(y)dy = \begin{cases} 0, & i \neq j \\ N_i, & i = j \end{cases}; \qquad N_i = \int_0^L \psi_i^2(y)dy = \frac{L}{2} \tag{12c-e}$$

$$\tilde{\psi}_i(y) = \frac{\psi_i(y)}{\sqrt{N_i}} \tag{12f}$$

The eigenvalue problem above allows the definition of the following integral transform pairs:

$$\bar{u}_{h,i}(t) = \int_0^L \tilde{\psi}_i(y)u_h(y,t)dy, \text{ transform;} \qquad u_h(y,t) = \sum_{i=1}^{\infty} \tilde{\psi}_i(y)\bar{u}_{h,i}(t), \quad \text{inverse} \tag{13a,b}$$

$$\bar{\omega}_{h,i}(t) = \int_0^L \tilde{\psi}_i(y)\omega_h(y,t)dy, \quad \text{transform;} \qquad \omega_h(y,t) = \sum_{i=1}^{\infty} \tilde{\psi}_i(y)\bar{\omega}_{h,i}(t), \quad \text{inverse} \tag{14a,b}$$

$$\bar{\theta}_{h,i}(t) = \int_0^L \tilde{\psi}_i(y)\theta_h(y,t)dy, \text{ transform;} \qquad \theta_h(y,t) = \sum_{i-1}^{\infty} \tilde{\psi}_i(y)\bar{\theta}_{h,i}(t), \quad \text{inverse} \tag{15a,b}$$

$$\bar{\phi}_{h,i}(t) = \int_0^L \tilde{\psi}_i(y)\phi_h(y,t)dy, \text{ transform;} \qquad \phi_h(y,t) = \sum_{i=1}^{\infty} \tilde{\psi}_i(y)\bar{\phi}_{h,i}(t), \quad \text{inverse} \tag{16a,b}$$

The process of integral transformation is now accomplished by multiplying Eqs. (6) and the initial conditions given by Eqs. (7a–d) with the normalized eigenfunctions $\psi_i(y)/N_i^{1/2}$ and integrated over the domain [0,*L*] in the *y* direction and the inverse formulae given by Eqs. (13–16b) are employed. Also, after the usual manipulations, the following coupled ordinary differential system is obtained:

$$\frac{d\bar{u}_{h,i}(t)}{dt} = \sum_{j=1}^{\infty} A_{ij}\bar{u}_{h,j}(t) - \left[\mu_i^2(1+\beta) + M + \frac{1+\beta}{K_1}\right]\bar{u}_{h,i}(t) + G_{rT}\bar{\theta}_{h,i}(t) + G_{rC}\bar{\phi}_{h,i}(t) + 2\beta\sum_{j=1}^{\infty} A_{ij}\bar{\omega}_{h,j}(t) + 2\beta\int_0^L \tilde{\psi}_i(y)\frac{\partial\omega_p}{\partial y}dy + G_{rT}\int_0^L \tilde{\psi}_i(y)\theta_p dy + G_{rC}\int_0^L \tilde{\psi}_i(y)\phi_p dy \tag{17a}$$

$$\frac{d\bar{\omega}_{h,i}(t)}{dt} = \sum_{j=1}^{\infty} A_{ij}\bar{\omega}_{h,j}(t) - \frac{\mu_i^2}{\eta}\bar{\omega}_{h,i}(t) - \int_0^L \tilde{\psi}_i(y)\frac{\partial\omega_p}{\partial t}dy \tag{17b}$$

$$\frac{d\bar{\theta}_{h,i}(t)}{dt} = \sum_{j=1}^{\infty} A_{ij}\bar{\theta}_{h,j}(t) - \frac{\mu_i^2}{Pr}\bar{\theta}_{h,i}(t) - \int_0^L \tilde{\psi}_i(y)\frac{\partial\theta_p}{\partial t}dy \tag{17c}$$

$$\frac{d\bar{\phi}_{h,i}(t)}{dt} = \sum_{j=1}^{\infty} A_{ij}\bar{\phi}_{h,j}(t) + \left(-\frac{\mu_i^2}{Sc} + \gamma_1\right)\bar{\phi}_{h,i}(t) - \int_0^L \tilde{\psi}_i(y)\frac{\partial\phi_p}{\partial t}dy \tag{17d}$$

$$\bar{u}_{h,i}(0) = \int_0^L \tilde{\psi}_i(y)F_1(y)dy; \qquad \bar{\omega}_{h,i}(0) = \int_0^L \tilde{\psi}_i(y)F_2(y)dy \tag{18a, b}$$

$$\bar{\theta}_{h,i}(0) = \int_0^L \tilde{\psi}_i(y)F_3(y)dy; \qquad \bar{\phi}_{h,i}(0) = \int_0^L \tilde{\psi}_i(y)F_4(y)dy \tag{18c, d}$$

With the following integral coefficient:

$$A_{ij} = \int_0^L \tilde{\psi}_i(y)\frac{d\tilde{\psi}_j(y)}{dy}dy \tag{19}$$

Eqs. (17a–d) form a coupled system of ordinary differential equations (ODE) that needs to be solved numerically by appropriate routines for this purpose, such as NDSolve from the symbolic numerical platform *Mathematica* 9.0 (Wolfram, 2005).

3.3. Method of lines (MOL)

The MOL replaces the spatial (boundary-value) derivatives in the PDE with algebraic approximations. Once this is done, the spatial derivatives are no longer stated explicitly in terms of the spatial independent variables. Thus, in effect, only the initial-value variable, typically time in a physical problem, remains. In other words, with only one remaining independent variable, it has a system of ODEs that approximates the original PDE. Once this is done, NDSolve can be used again to solve the system of ODEs. Thus, one of the salient features of the MOL is the use of existing, and generally well-established, numerical methods for ODEs (Schiesser and Griffiths, 2009).

Employing an approximation for the derivatives, the following ODE system is generated:

$$\frac{du_i(t)}{dt} = u_{i+1}(t)\left(\frac{1}{2\Delta y} + \frac{1+\beta}{\Delta y^2}\right) - u_i(t)\left[\frac{2(1+\beta)}{\Delta y^2} + M + \frac{1+\beta}{K_1}\right] + u_{i-1}(t)\left(\frac{1+\beta}{\Delta y^2} - \frac{1}{2\Delta y}\right) + 2\beta\left[\frac{\omega_{i+1}(t) - \omega_{i-1}(t)}{2\Delta y}\right] + G_{rT}\theta_i(t) + G_{rC}\phi_i(t) \tag{20a}$$

$$\frac{d\omega_i(t)}{dt} = \omega_{i+1}(t)\left(\frac{1}{2\Delta y} + \frac{\eta^{-1}}{\Delta y^2}\right) - \omega_i(t)\left(\frac{2\eta^{-1}}{\Delta y^2}\right) + \omega_{i-1}(t)\left(\frac{\eta^{-1}}{\Delta y^2} - \frac{1}{2\Delta y}\right) \tag{20b}$$

$$\frac{d\theta_i(t)}{dt} = \theta_{i+1}(t)\left(\frac{1}{2\Delta y} + \frac{Pr^{-1}}{\Delta y^2}\right) - \theta_i(t)\left(\frac{2Pr^{-1}}{\Delta y^2}\right) + \theta_{i-1}(t)\left(\frac{Pr^{-1}}{\Delta y^2} - \frac{1}{2\Delta y}\right) \tag{20c}$$

$$\frac{d\phi_i(t)}{dt} = \phi_{i+1}(t)\left(\frac{1}{2\Delta y} + \frac{Sc^{-1}}{\Delta y^2}\right) - \phi_i(t)\left(\frac{2Sc^{-1}}{\Delta y^2} - \gamma_1\right) + \phi_{i-1}(t)\left(\frac{Sc^{-1}}{\Delta y^2} - \frac{1}{2\Delta y}\right) \tag{20d}$$

With the initial and boundary conditions as follows:

$$\begin{cases} u_i(0) = f_1(y_i,0) \\ \omega_i(0) = f_2(y_i,0) \\ \theta_i(0) = f_3(y_i,0) \\ \phi_i(0) = f_4(y_i,0) \end{cases}; \quad \begin{cases} u_1(t) = U_p \\ \omega_1(t) = -n_1 \frac{u_2(t)-u_1(t)}{\Delta y}\Big|_{y=0} \\ \theta_1(t) = 1 + \varepsilon e^{nt} \\ \phi_1(t) = 1 + \varepsilon e^{nt} \end{cases}; \quad \begin{cases} u_{NPT}(t) = 0 \\ \omega_{NPT}(t) = 0 \\ \theta_{NPT}(t) = 0 \\ \phi_{NPT}(t) = 0 \end{cases} \tag{21a-l}$$

3.4. Engineering parameters

The local skin friction coefficient, local wall couple stress coefficient, local Nusselt number and local Sherwood number are important physical quantities for this type of heat and mass transfer problem. These are defined by Modather et al. (2009) as follows:

- Local skin friction factor:

$$C_f = \frac{2\tau_w^*}{\rho U_0 V_0} = 2[1 + (1 - n_1)\beta]u'(0) \tag{22}$$

where the wall shear stress may be written as:

$$\tau_w^* = (\mu + \Lambda)\frac{\partial u^*}{\partial y^*}\Big|_{y^*=0} + \Lambda\omega^*|_{y^*=0} = \rho U_0 V_0[1 + (1 - n_1)\beta]u'(0) \tag{23}$$

- Local couple stress coefficient:

$$C'_w = \frac{M_w \nu^2}{\gamma U_0 V_0^2} = \omega'(0) \tag{24}$$

where the wall couple stress may be written as:

$$M_w = \gamma\frac{\partial \omega^*}{\partial y^*}\Big|_{y^*=0} \tag{25}$$

- Heat transfer rate at the surface in terms of the local Nusselt number:

$$NuRe_x^{-1} = -\theta'(0) \tag{26}$$

- Mass transfer rate at the surface in terms of the local Sherwood number:

$$ShRe_x^{-1} = -\phi'(0) \tag{27}$$

where the local Nusselt number, the local Sherwood number and the local Reynolds number are defined as follows:

$$Nu = x\frac{\partial T/\partial y^*|_{y^*=0}}{T_\infty - T_w} \tag{28}$$

$$Sh = x\frac{\partial C/\partial y^*|_{y^*=0}}{C_\infty - C_w} \tag{29}$$

$$Re_x = xV_0/\nu \tag{30}$$

3.5. Recovering the original potentials

The original potentials and some related quantities can be evaluated from their definitions using the inversion formulae given by Eqs. (13–16b) together with the respective particular solutions:

- Linear velocity field:

$$u(y,t) = u_p(y) + u_h(y,t) = u_p(y) + \sum_{i=1}^{\infty}\tilde{\psi}_i(y)\bar{u}_{h,i}(t) \tag{31a}$$

- Angular velocity field:

$$\omega(y,t) = \omega_p(y;t) + \omega_h(y,t) = \omega_p(y;t) + \sum_{i=1}^{\infty}\tilde{\psi}_i(y)\bar{\omega}_{h,i}(t) \tag{31b}$$

- Temperature field:

$$\theta(y,t) = \theta_p(y;t) + \theta_h(y,t) = \theta_p(y;t) + \sum_{i=1}^{\infty}\tilde{\psi}_i(y)\bar{\theta}_{h,i}(t) \tag{31c}$$

- Concentration field:

$$\phi(y,t) = \phi_p(y;t) + \phi_h(y,t) = \phi_p(y;t) + \sum_{i=1}^{\infty}\tilde{\psi}_i(y)\bar{\phi}_{h,i}(t) \tag{31d}$$

4. Results and discussion

To obtain numerical results from the coupled system of ordinary differential equations, Eqs. (17) and (20), two methodologies were applied: the eigenfunction expansions were truncated to a finite number of terms N, which is the truncation order of the recovered potential in the GITT approach and discretization of the system with a number of points, NPT, in the mesh using approximation formulas in the MOL solution. Therefore, N and NPT were assigned to the NDSolve subroutine from the numerical-symbolic computing platform *Mathematica 9.0* (2005). While not explicitly shown in the text, the results shown were obtained by adopting $N = 580$ and $NPT = 800$, numbers high enough to guarantee the convergence of all fields for the various situations analyzed.

4.1. Convergence behavior analysis and verification of results

Convergence analysis of the linear and angular velocity components, the temperature and the concentration fields, i.e., gradually increasing the truncation order of the GITT expansions until a certain criterion of numerical error in the analyzed fields is reached. Such analysis it was performed to illustrate the main numerical features of the present approach at certain positions along the plate.

Tables 1 and 2 illustrate the convergence behavior of the GITT solution for two different dimensionless times, $t = 1$ and $t = 50$, respectively, using the parameters K_1=5, γ_1=0.1, $\varepsilon = 0.01$, n_1=0.5, $n = 0.1$, $\beta = 1$, $M = 2$, G_{rT}=2, G_{rC}=1, $Pr = 1$, $Sc = 2$ and $U_p = 0.5$.

According to these tables, with 20 terms in the series the temperature and concentration fields are already substantially converged within four digits, even at flow regions very close to the plate entry ($y = 0.5$). In contrast, despite the temperature and concentration fields requiring fewer than 20 terms to converge, the linear and angular velocity fields need more than 580 terms for a convergence to four digits in both cases ($t = 1$ and $t = 50$). It is noticed that the linear and angular velocity fields did not significantly change for the two dimensionless times analyzed, although for short time ($t = 1$) the temperature and concentration fields converged with fewer terms in the series ($N = 20$) when compared to $t = 50$ in which the convergence required $N = 60$.

The transient behavior of the linear and angular velocities, temperature and concentration profiles is observed in Fig. 2a–d, which is performed for the dimensionless times $t = 0$, 30, 40 and 50. Also, from these figures, verification of results shows the excellent agreement between the calculated concentration field using the GITT approach with results of Modather et al. (2009), as well as with those of the MOL approach. However, the results of the

Table 1
Convergence behavior of the GITT results for linear and angular velocity components, temperature and concentration distribution at different axial positions for $t = 1$, $K_1 = 5$, γ_1=0.1, $\varepsilon = 0.01$, $n_1 = 0.5$, $n = 0.1$, $\beta = 1$, $M = 2$, $G_{rT} = 2$, $G_{rC} = 1$, $Pr = 1$, $Sc = 2$ and $U_p = 0.5$.

NT	u(y,t)					ω(y,t)				
	$y = 0.5$	$y = 1$	$y = 2$	$y = 3$	$y = 7$	$y = 0.5$	$y = 1$	$y = 2$	$y = 3$	$y = 7$
500	0.443770	0.331285	0.151791	0.062468	0.001100	−0.013317	−0.009461	−0.004788	−0.002449	−0.000115
520	0.443790	0.331309	0.151808	0.062477	0.001100	−0.013422	−0.009534	−0.004822	−0.002465	−0.000115
540	0.443809	0.331331	0.151824	0.062485	0.001101	−0.013520	−0.009601	−0.004854	−0.002480	−0.000116
560	0.443827	0.331352	0.151838	0.062493	0.001101	−0.013610	−0.009663	−0.004883	−0.002494	−0.000116
580	0.443843	0.331371	0.151852	0.062500	0.001101	−0.013694	−0.009721	−0.004911	−0.002507	−0.000117
MOL ($NPT = 800$)	0.442667	0.329636	0.150708	0.062095	0.001109	−0.011160	−0.008290	−0.004620	−0.002560	−0.000130
Modather et al. (2009)	0.444485	0.332242	0.152625	0.063018	0.001447	−0.016603	−0.012078	−0.006405	−0.003407	−0.000282
NT	θ(y,t)					ϕ(y,t)				
	$y = 0.5$	$y = 1$	$y = 2$	$y = 3$	$y = 7$	$y = 0.5$	$y = 1$	$y = 2$	$y = 3$	$y = 7$
20	0.613156	0.371920	0.136905	0.050421	0.000685	0.392004	0.152033	0.022882	0.003447	0.000003
40	0.613158	0.371920	0.136906	0.050420	0.000685	0.392011	0.152033	0.022884	0.003446	0.000002
60	0.613158	0.371920	0.136906	0.050420	0.000685	0.392011	0.152033	0.022884	0.003446	0.000002
80	0.613158	0.371920	0.136906	0.050420	0.000685	0.392011	0.152033	0.022884	0.003447	0.000002
100	0.613158	0.371920	0.136906	0.050420	0.000685	0.392011	0.152033	0.022884	0.003447	0.000002
MOL ($NPT = 800$)	0.618940	0.375190	0.137936	0.050736	0.000686	0.378882	0.139199	0.018802	0.002541	0.000000
Modather et al. (2009)	0.613622	0.372430	0.137209	0.050559	0.000934	0.392371	0.152278	0.022939	0.003456	0.000002

Table 2
Convergence behavior of the GITT results for linear and angular velocity components, temperature and concentration distribution at different axial positions for $t = 50$, $K_1 = 5$, γ_1=0.1, $\varepsilon = 0.01$, $n_1 = 0.5$, $n = 0.1$, $\beta = 1$, $M = 2$, $G_{rT} = 2$, $G_{rC} = 1$, $Pr = 1$, $Sc = 2$ and $U_p = 0.5$.

NT	u(y,t)					ω(y,t)				
	$y = 0.5$	$y = 1$	$y = 2$	$y = 3$	$y = 7$	$y = 0.5$	$y = 1$	$y = 2$	$y = 3$	$y = 7$
500	0.783094	0.694151	0.367333	0.162921	0.003696	−0.450585	−0.308911	−0.144951	−0.067690	−0.001923
520	0.783149	0.694218	0.367381	0.162950	0.003697	−0.450876	−0.309114	−0.145049	−0.067737	−0.001924
540	0.783200	0.694279	0.367427	0.162975	0.003698	−0.451146	−0.309302	−0.145140	−0.067781	−0.001925
560	0.783249	0.694336	0.367469	0.162999	0.003700	−0.451396	−0.309476	−0.145224	−0.067821	−0.001927
580	0.783293	0.694390	0.367508	0.163022	0.003701	−0.451629	−0.309638	−0.145302	−0.067859	−0.001928
MOL ($NPT = 800$)	0.775663	0.688526	0.364418	0.161668	0.003652	−0.445160	−0.304980	−0.142910	−0.066650	−0.001880
Modather et al. (2009)	0.837083	0.779444	0.456567	0.227404	0.012499	−0.550269	−0.418623	−0.242337	−0.140326	−0.015812
NT	θ(y,t)					ϕ(y,t)				
	$y = 0.5$	$y = 1$	$y = 2$	$y = 3$	$y = 7$	$y = 0.5$	$y = 1$	$y = 2$	$y = 3$	$y = 7$
20	1.465646	0.865754	0.301967	0.105526	0.001160	0.932639	0.351231	0.049472	0.007295	0.000243
40	1.466223	0.865717	0.302171	0.105442	0.001070	0.933810	0.351153	0.049855	0.007052	0.000002
60	1.466229	0.865768	0.302143	0.105454	0.001068	0.933831	0.351261	0.049789	0.007075	−0.000003
80	1.466202	0.865773	0.302152	0.105458	0.001071	0.933773	0.351271	0.049810	0.007085	0.000003
100	1.466219	0.865767	0.302148	0.105457	0.001072	0.933809	0.351258	0.049800	0.007082	0.000004
MOL ($NPT = 800$)	1.480788	0.873786	0.304542	0.106151	0.001073	0.905699	0.32366	0.041402	0.005308	0.000000
Modather et al. (2009)	1.558884	0.978995	0.386972	0.153403	0.003891	0.998936	0.402042	0.065287	0.010636	0.000008

calculations of the other fields do not agree with the literature results at longer times ($t = 30$, 40 and 50). This is due to the fact that the solution methodology employed by Modather et al. (2009) is an approximation. Thus, the integral transform results may be considered closest to the actual behavior of the flow for longer time, since these results agreed with the MOL results.

As seen in Fig. 2a–d, the fluid velocity, temperature and the solute concentration in the fluid increase as time increases, while the angular velocity of the fluid decreases with increasing time. Furthermore, the velocity increases with time. The velocity profiles achieve a maximum value near the surface, and approach an asymptotic value (free stream velocity) with increasing distance from the surface. In addition, the momentum boundary layer thickness increases as t increases. The thermal boundary layer thickness decreases and the temperature gradient at the wall increases as t decreases. Hence, the heat transfer rate increases as t decreases. The temperature is high near the surface of the plate and decreases with increasing distance from the plate, approaching an asymptotic value

The following section studies the effect of the variation of the system parameters on the linear and angular velocity, temperature and concentration fields. The parameters employed in the present analysis were:

- Magnetic field parameter (M): which is directly proportional to the magnetic field applied externally, B_0, Eq. (3n);
- Schmidt number (Sc): describes the relative thickness of the velocity and the mass boundary layers. It is the relation between the viscous diffusion rate, ν, and the species diffusion rate, D, Eq. (3m);
- Prandtl number (Pr): describes the relative thickness of the velocity and the thermal boundary layers. It is the relation between the viscous diffusion rate, ν, and the heat diffusion rate, α, Eq. (3l);
- Permeability parameter (K_1): which is directly proportional to the porosity of the media, K. The presence of a porous medium provides an increase in flow resistance, Eq. (3s);
- Chemical reaction parameter (γ_1): which is directly proportional to the reaction rate constant, γ_1^*, Eq. (3t).

4.2. Effect of magnetic field parameter

Fig. 3a and b show the sensitivity of the linear and angular velocities to the magnetic field parameter (M). The examination is performed for $M = 0$, 2, 3 and 4. From these figures, it is shown that the linear velocity decreases with increasing magnetic field intensity, while the angular velocity increases with increasing M.

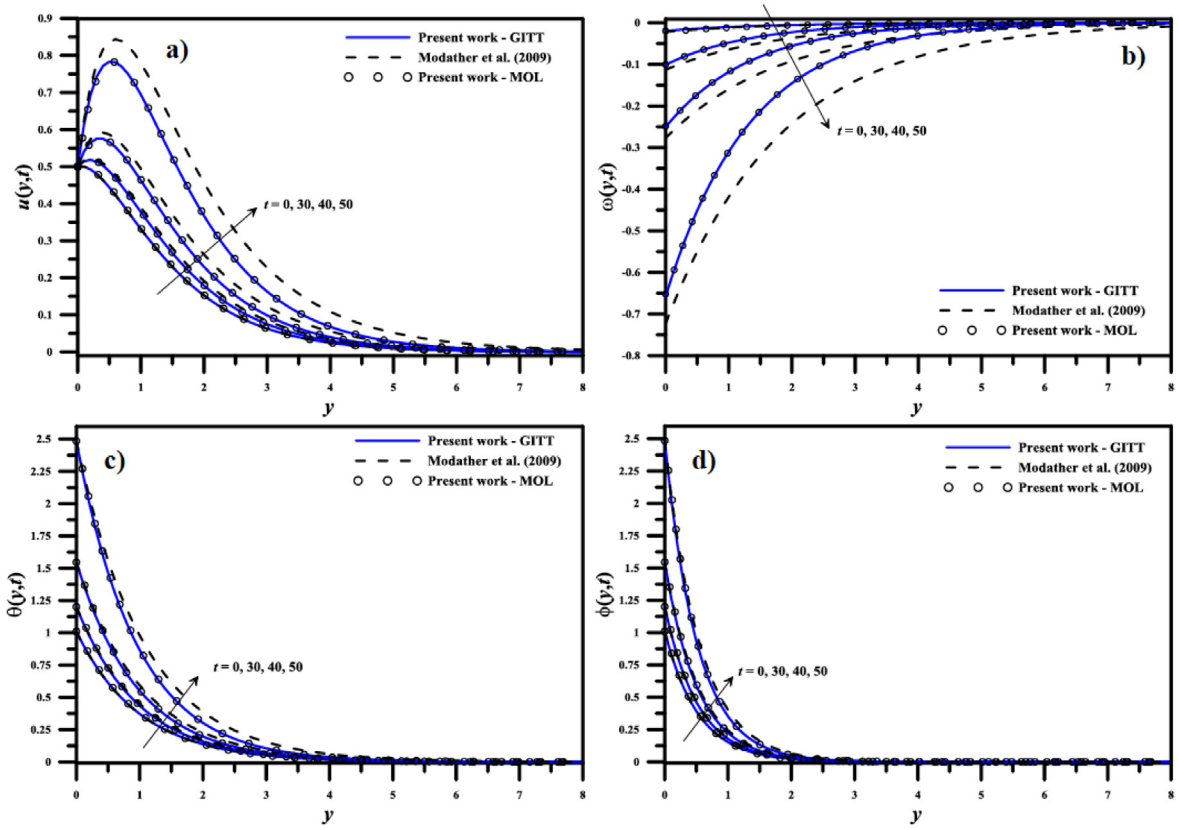

Fig. 2. Transient behavior of the potential distributions for $K_1 = 5$, γ_1=0.1, $\varepsilon = 0.01$, $n_1 = 0.5$, $n = 0.1$, $\beta = 1$, $M = 2$, $G_{rT} = 2$, $G_{rC} = 1$, $Pr = 1$, $Sc = 2$ and $U_p = 0.5$: a) linear velocity; b) angular velocity; c) temperature; d) concentration.

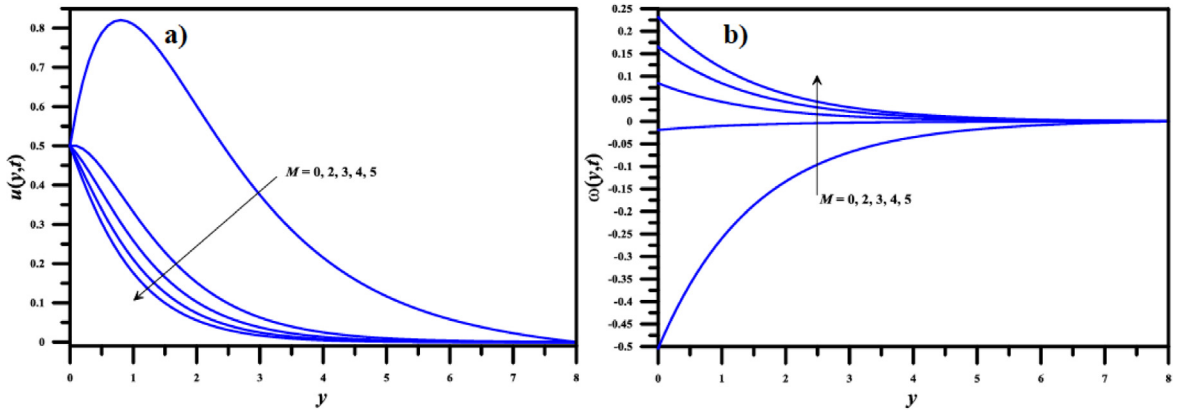

Fig. 3. Effect of magnetic field parameter (M) on the potential distributions for $t = 1$, $K_1 = 5$, γ_1=0.1, $\varepsilon = 0.01$, $n_1 = 0.5$, $n = 0.1$, $\beta = 1$, $G_{rT} = 2$, $G_{rC} = 1$, $Pr = 1$ and $U_p = 0.5$: a) linear velocity; b) angular velocity.

The application of a magnetic field to an electrically conductive fluid produces a resistive force to flow (Lorentz force), slowing the movement of the fluid.

4.3. Effect of Schmidt number

The influence of the Schmidt number on the linear and angular velocities and concentration field is illustrated in Fig.4a–c. The investigation is performed for $Sc = 1$, 2, 3 and 5. There, it is observed that the linear and angular velocities and the concentration field decrease as the Schmidt number increases. For $Sc = 2$ the viscous diffusion rate (ν) is twice the value of the species diffusion rate (D); thus, the velocity and the concentration are larger than the results for $Sc = 5$ where the viscous diffusion rate is five times larger than the species diffusion rate.

4.4. Effect of Prandtl number

Fig. 5a–c illustrate the influence of the Prandtl number on the linear and angular velocities and temperature field for $Pr = 0.71$, 1, 3 and 7. As shown in these figures, the linear velocity and the temperature decrease as Pr is increased, while the angular velocity increases with the Prandtl number. When $Pr = 0.71$ (air at 20 °C) the viscous diffusion rate (ν) is lower than the heat diffusion rate (α) and thus the velocity and temperature are lower when compared to the results of $Pr = 1$ (electrolytic solution) where ν is equal

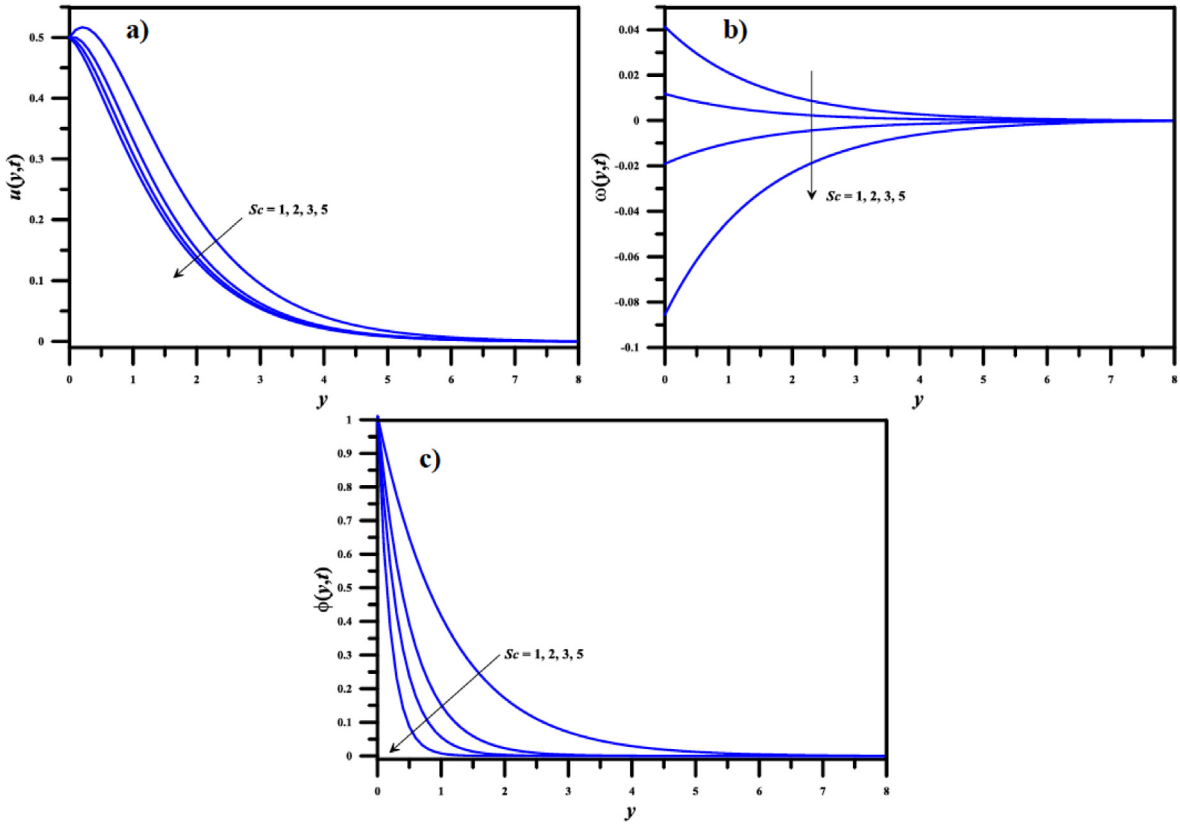

Fig. 4. Effect of Schmidt number (Sc) on the potential distributions for $t = 1$, $K_1 = 5$, γ_1=0.1, $\varepsilon = 0.01$, $n_1 = 0.5$, $n = 0.1$, $\beta = 1$, $M = 2$, $G_{rT} = 2$, $G_{rC} = 1$, $Pr = 1$ and $U_p = 0.5$: a) linear velocity; b) angular velocity; c) concentration.

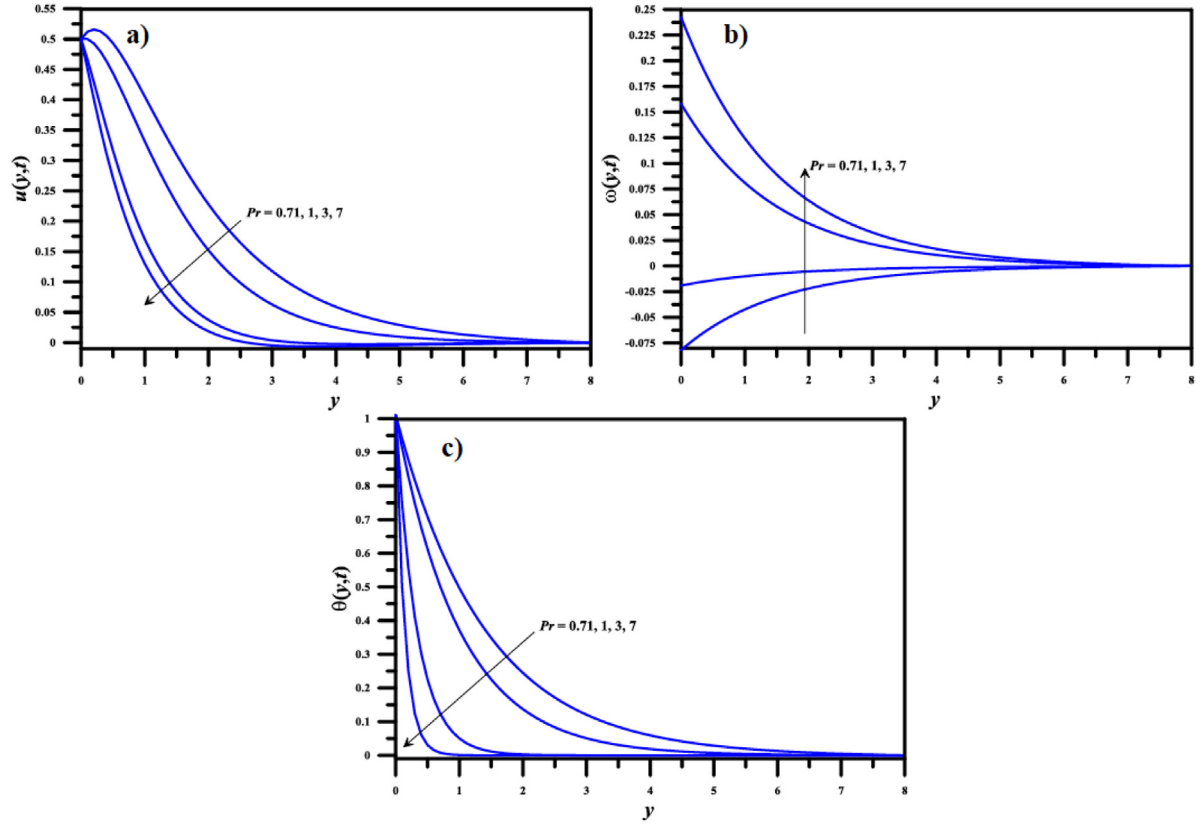

Fig. 5. Effect of Prandtl number (Pr) on the potential distributions for $t = 1$, $K_1 = 5$, γ_1=0.1, $\varepsilon = 0.01$, $n_1 = 0.5$, $n = 0.1$, $\beta = 1$, $M = 2$, $G_{rT} = 2$, $G_{rC} = 1$, $Sc = 2$ and $U_p = 0.5$: a) linear velocity; b) angular velocity; c) temperature.

in order of magnitude to α. For $Pr = 3$ and $Pr = 7$ (water), where the viscous diffusion rate is larger than the heat diffusion rate, the temperatures are much lower when compared to the results from the other values of Prandtl number.

4.5. Effect of permeability parameter

Fig. 6a and b show the influence of the permeability parameter (K_1) on the linear and angular velocities and temperature field for K_1=1, 2, 3, 4, 5 and ∞ (taken 10,000). As the permeability parameter (K_1) increases, the linear velocity increases along with the thickness of the boundary layer, while the angular velocity decreases. The presence of a porous medium increases flow resistance (i.e., as K_1 decreases), so that the resulting resistive force tends to reduce the movement of fluid along the plate surface and promotes an increase in angular velocity.

4.6. Effect of chemical reaction parameter

Fig. 7a–c show the influence of the chemical reaction parameter (γ_1) on the linear and angular velocities and concentration field for γ_1=0, 0.1, 0.2, 0.3 and 0.4. The linear velocity and the concentration increase as γ_1 increases, while the angular velocity has the opposite behavior, although it should be emphasized that γ_1 has little influence on the linear velocity field.

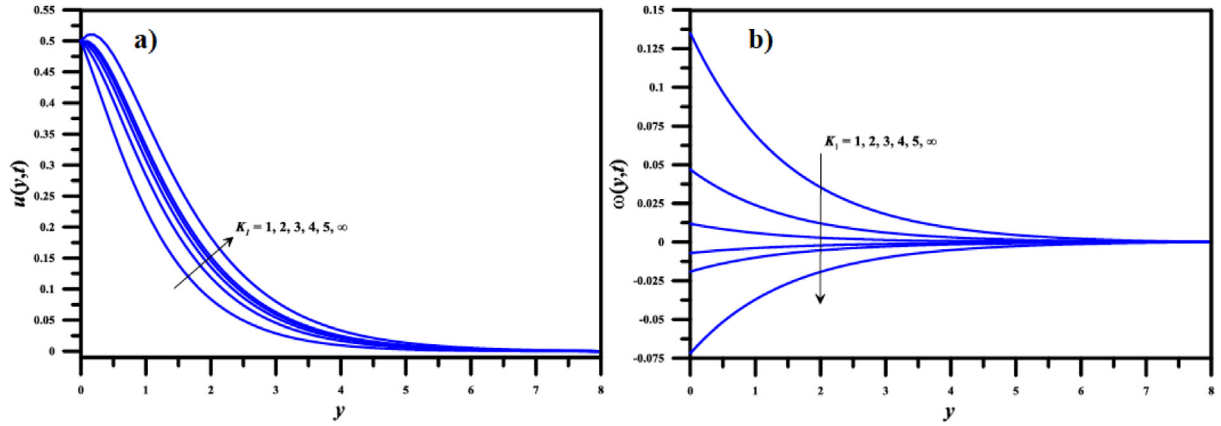

Fig. 6. Effect of permeability parameter (K_1) on the potential distributions for $t = 1$, $\varepsilon = 0.01$, $n_1 = 0.5$, $n = 0.1$, $\beta = 1$, $M = 2$, $G_{rT} = 2$, $G_{rC} = 1$, $Pr = 1$, $Sc = 2$ and $U_p = 0.5$: a) linear velocity; b) angular velocity.

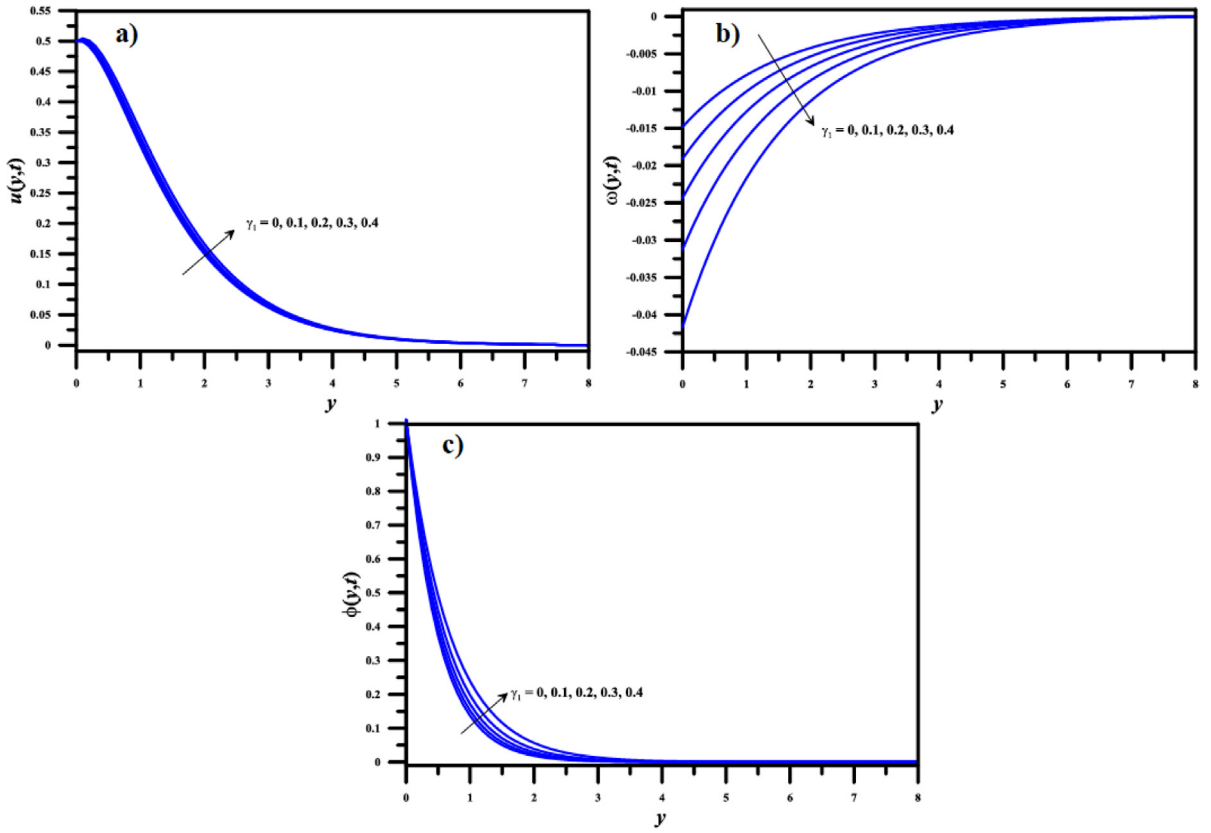

Fig. 7. Effect of chemical reaction parameter (γ_1) on the potential distributions for $t = 1$, $K_1 = 5$, $\varepsilon = 0.01$, $n_1 = 0.5$, $n = 0.1$, $\beta = 1$, $M = 2$, $G_{rT} = 2$, $G_{rC} = 1$, $Pr = 1$, $Sc = 2$ and $U_p = 0.5$: a) linear velocity; b) angular velocity; c) concentration.

Table 3
Effects of variations of chemical reaction and permeability parameters on the coefficients of skin friction, couple stress, heat transfer and mass transfer for $t = 1$, $\varepsilon = 0.01$, $n_1 = 0.5$, $n = 0.1$, $\beta = 1$, $M = 2$, $G_{rT} = 2$, $G_{rC} = 1$, $Pr = 1$, $Sc = 2$ and $U_p = 0.5$.

γ_1	K_1	C_f	C'_w	$NuRe_x^{-1}$	$ShRe_x^{-1}$
0	1	−0.81371	−0.09106	1.00643	2.00278
	2	−0.28897	−0.03366		
	3	−0.08012	−0.0108		
	5	0.104194	0.009396		
	∞	0.418018	0.043796		
0.1	1	−0.79383	−0.08887	1.00643	1.89808
	2	−0.26594	−0.03112		
	3	−0.05572	−0.0081		
	5	0.129858	0.012227		
	∞	0.445951	0.046876		
0.2	1	−0.76954	−0.08619	1.00643	1.77907
	2	−0.23766	−0.02801		
	3	−0.0257	−0.00479		
	5	0.161488	0.015715		
	∞	0.480476	0.050683		

4.7. Effect of parameters on C_f, C'_w, $NuRe_x^{-1}$ and $ShRe_x^{-1}$

Table 3 illustrates the effects of the chemical reaction parameter, γ_1, and the permeability parameters, K_1, on the coefficients of skin friction, couple stress, heat transfer and mass transfer. It can be seen that as K_1 increases, both C_f and C'_w increase. For increasing γ_1, both C_f and C'_w increase, while $ShRe_x^{-1}$ decreases as the chemical reaction parameter increases.

Table 4
Unsteady behaviors of the coefficients of skin friction, couple stress, heat transfer and mass transfer with various values of t for $K_1 = 5$, γ_1=0.1, $\varepsilon = 0.01$, $n_1 = 0.5$, $n = 0.1$, $\beta = 1$, $M = 2$, $G_{rT} = 2$, $G_{rC} = 1$, $Pr = 1$, $Sc = 2$ and $U_p = 0.5$.

t	C_f	C'_w	$NuRe_x^{-1}$	$ShRe_x^{-1}$
0	0.13379	−0.33944	1.003844	1.894163
1	0.129858	0.012227	1.00643	1.898082
3	0.136421	0.013787	1.009512	1.903274
5	0.144142	0.014956	1.012986	1.90926
10	0.171954	0.018567	1.024827	1.930465
20	0.294258	0.033806	1.075582	2.022959
30	0.626805	0.075172	1.213436	2.274371
40	1.530762	0.187615	1.588161	2.95778
50	3.987973	0.493268	2.60677	4.815479

Table 4 presents the variation of the coefficients of skin friction, couple stress, heat transfer and mass transfer for different dimensionless times. In general, skin friction, couple stress, heat transfer and mass transfer increase with time.

Table 5 presents the effects of Pr, Sc, G_{rT}, G_{rC}, n_1, n, β, ε, U_p and M on skin friction and couple stress across the boundary layer, as well as the local Nusselt and Sherwood numbers. It can be concluded that the skin friction and the couple stress decrease as the plate velocity, U_p, and magnetic parameter, M, increase. It can also note from this table that increasing Pr, G_{rT}, G_{rC}, n_1, n or ε causes C_f and C'_w to increase, while increasing Sc or β produces lower values of C_f and C'_w. On the other hand, the local Nusselt number increases as n, Pr or ε increase and the local Sherwood number increases as n, Sc or ε increase.

Table 5
Effects of variations of flow conditions and fluid properties on the coefficients of skin friction, couple stress, heat transfer and mass transfer for $t = 1$, $K_1 = 5$, γ_1=0.1, $\varepsilon = 0.01$, $n_1 = 0.5$, $n = 0.1$, $\beta = 1$, $M = 2$, $G_{rT} = 2$, $G_{rC} = 1$, $Pr = 1$, $Sc = 2$ and $U_p = 0.5$.

		C_f	C'_w	$NuRe_x^{-1}$	$ShRe_x^{-1}$
Pr	0.71	0.507916	0.053958	0.715516	1.89808
	1	0.129858	0.012227	1.00643	
Sc	1	0.529522	0.056338	1.00643	0.893247
	2	0.129858	0.012227		1.89808
G_{rT}	0	−1.92717	−0.21271		1.89808
	1	−0.89866	−0.10024		
	2	0.129858	0.012227		
G_{rC}	0	−0.56531	−0.06344		
	1	0.129858	0.012227		
	2	0.825031	0.08789		
n_1	0	0.14121	0		
	0.5	0.129858	0.012227		
	1	0.113438	0.033266		
n	0	0.127621	0.01205	1.00497	1.89539
	0.05	0.128725	0.012159	1.00569	1.8967
	0.1	0.129858	0.012227	1.00643	1.89808
	0.15	0.130877	0.012149	1.00716	1.89953
β	0	0.575446	0.137349	1.00643	1.89808
	1	0.129858	0.012227		
	1.5	−0.08273	−0.00824		
ε	0	0.100393	0.009076	0.995016	1.87663
	0.01	0.129858	0.012227	1.00643	1.89808
	0.1	0.395046	0.040586	1.10916	2.09118
U_p	0	2.75221	0.300596	1.00643	1.89808
	0.5	0.129858	0.012227		
	1	−2.49249	−0.27614		
M	0	3.04355	0.33213		
	2	0.129858	0.012227		
	3	−0.4929	−0.05596		
	4	−0.97399	−0.10855		

5. Conclusions

The present work has analyzed the unsteady one-dimensional MHD oscillatory flow of a micropolar and incompressible fluid with heat and mass transfer through a permeable vertical plate embedded in a porous medium in the presence of chemical reaction using the GITT approach as solution methodology for the related governing equations.

In the results, it was observed that the angular velocity increases with increasing magnetic field intensity, while the linear velocity decreases with increasing the same. The linear and angular velocities and the concentration field decrease as the Schmidt number increases. It is also observed that the linear velocity and the temperature decrease as Prandtl number is increased, while the angular velocity increases with this parameter.

The results obtained with the GITT approach compare reasonably with the literature results and very well with those obtained using the MOL approach. Therefore, the computer code developed in this study was employed for an in-depth investigation of the effects of governing parameters on the flow, heat transfer and mass transfer over the plate.

The hybrid GITT approach proved to be a versatile method for the solution of the nonlinear problem examined in this work, therefore enabling the study of the class of problems that involve electromagnetic phenomena combined with heat and mass transfer in the presence of chemical reaction.

It is remarkable that there are no previous studies addressing the solution of micropolar fluid MHD flow models by the GITT method. Therefore, the present work represents an expansion of the application of the present methodology and can be extended to analyze other effects, such as radiation and viscous dissipation in the governing equations.

References

Acharya, A.K., Dash, G.C., Mishra, S.R., 2014. Free convective fluctuating MHD flow through porous media past a vertical porous plate with variable temperature and heat source. Phys. Res. Int. 2014. Article ID 587367.

Al-Odat, M.Q., Al-Azab, T.A., 2007. Influence of chemical reaction on transient MHD free convection over a moving vertical plate, Emirates. J. Eng. Res. 12, 15–21.

Ansys, C.F.X., 2009. Reference Manual. Ansys Inc., USA.

Babu, M.S., Kumar, J.G., Reddy, T.S., 2013. Mass transfer effects on unsteady MHD convection flow of micropolar fluid past a vertical moving porous plate through porous medium with viscous dissipation. Int. J. Appl. Math. Mech. 9, 48–67.

Bég, O.A., Ferdows, M., Bég, E.T.A., Ahmed, T., Wahiduzzaman, M., Alam, Md.M., 2016. Numerical investigation of radiative optically-dense transient magnetized reactive transport phenomena with cross diffusion, dissipation and wall mass flux effects. J. Taiwan Inst. Chem. Eng. 66, 12–26.

Cotta, R.M., 1993. Integral Transform in Computational Heat and Fluid Flow. CRC Press, Boca Raton, USA.

Cotta, R.M., Mikhailov, M.D., 1997. Heat Conduction: Lumped Analysis, Integral Transforms, Symbolic Computation. John Wiley & Sons, Chichester, England.

Davidson, P.A., 2001. An Introduction to Magnetohydrodynamics. Cambridge University Press, Cambridge, UK.

Eringen, A.C., 1966. Theory of micropolar fluids. J. Math. Mech. 16, 1–16.

Gupta, D., Kumar, L., Singh, B., 2014. Finite element solution of unsteady mixed convection flow of micropolar fluid over a porous shrinking sheet. Sci. World J. 2014. article ID 362351.

Lima, J.A., Rêgo, M.G.O., 2013. On the integral transform solution of low-magnetic MHD flow and heat transfer in the entrance region of a channel. Int. J. Non-Linear Mech. 50, 25–39.

Lima, J.A., Quaresma, J.N.N., Macêdo, E.N., 2007. Integral transform analysis of MHD flow and heat transfer in parallel-plates channels. Int. Commun. Heat Mass Transfer 34, 420–431.

Modather, M., Rashad, A.M., Chamkha, A.J., 2009. An analytical study of MHD heat and mass transfer oscillatory flow of a micropolar fluid over a vertical permeable plate in a porous medium. Turk. J. Eng. Environ. Sci. 33, 245–257.

Özisik, M.N., 1993. Heat Conduction. John Wiley & Sons, New York.

Pal, D., Talukdar, B., 2010a. Perturbation analysis of unsteady magnetohydrodynamic convective heat and mass transfer in a boundary layer slip flow past a vertical permeable plate with thermal radiation and chemical reaction. Commun. Nonlinear Sci. Numer. Simul. 15, 1813–1830.

Pal, D., Talukdar, B., 2010b. Buoyancy and chemical reaction effects on MHD mixed convection heat and mass transfer in a porous medium with thermal radiation and Ohmic heating. Commun. Nonlinear Sci. Numer. Simul. 15, 2878–2893.

Prasad, K.V., Vajravelu, K., Sujatha, A., 2013. Influence of internal heat generation/absorption, thermal radiation, magnetic field, variable fluid property and viscous dissipation on heat transfer characteristics of a Maxwell fluid over a stretching sheet. J. Appl. Fluid Mech. 6, 249–256.

Santos, C.A.C., Quaresma, J.N.N., Lima, J.A., 2001. Convective Heat Transfer in Ducts: The Integral Transform Approach, E-Papers, ABCM Mechanical Sciences Series, Rio de Janeiro, Brazil.

Schiesser, W.E., Griffiths, G.W., 2009. A Compendium of Partial Differential Equation Models: Method of Lines Analysis with Matlab. Cambridge University Press, New York.

Sheikh, N.A., Ali, F., Khan, I., Saqib, M., Khan, A., 2017. MHD flow of micropolar fluid over an oscillating vertical plate embedded in porous media with constant temperature and concentration. Math. Prob. Eng. 2017, 20p.

Shercliff, J.A., 1965. A Textbook of Magnetohydrodynamics. Pergamon Press, London, UK.

Sphaier, L.A., Cotta, R.M., Naveira-Cotta, C.P., Quaresma, J.N.N., 2011. The UNIT algorithm for solving one-dimensional convection-diffusion problems via integral transforms. Int. Commun. Heat Mass Transfer 38, 565–571.

Sutton, G.W., Sherman, A., 2006. Engineering Magnetohydrodynamics. Dover Publications, New York, USA.

Vija, A.G., Rushi Kumar, B., Reddappa, B., Raveendra Babu, K., Varma, S.V.K., 2014. The effects of induced magnetic field and viscous dissipation on MHD mixed convective flow past a vertical plate in the presence of thermal radiation. Int. J. Appl. Eng. Res. 9, 4533–4547.

Wolfram, S., 2005. Mathematica: A System for doing Mathematics by Computer. Addison Wesley, Reading, MA.